When Soft Crystals Defy Newton's Third Law: Nonreciprocal Mechanics and Dislocation Motility

Alexis Poncet* and Denis Bartolo†
Université Lyon, ENS de Lyon, Université Claude Bernard, CNRS, Laboratoire de Physique, F-69342 Lyon, France

(Received 10 June 2021; revised 7 October 2021; accepted 23 December 2021; published 24 January 2022)

The effective interactions between the constituents of driven soft matter generically defy Newton's third law. Combining theory and numerical simulations, we establish that six classes of mechanics with no counterparts in equilibrium systems emerge in elastic crystals challenged by nonreciprocal interactions. Going beyond linear deformations, we reveal that interactions violating Newton's third law generically turn otherwise quiescent dislocations into motile singularities which steadily glide though periodic lattices.

DOI: 10.1103/PhysRevLett.128.048002

The constituents of driven soft matter interact via effective forces which are generically nonreciprocal. These constituents escape the elementary constraints imposed by Newton's third law by constantly exchanging linear and angular momentum with their surrounding medium. Hydrodynamic interactions provide a paradigmatic example of such nonreciprocal interactions [1]. Take the minimal system involving two identical colloidal particles A and B sedimenting in a viscous fluid, the drag force acting on B due to the motion of A is never opposite to the drag force acting on A due to the motion of B, whatever the relative position of the two particles, see Fig. 1(a). In a colloidal suspension these nonreciprocal interactions result in complex chaotic trajectories at odds with the homogeneous and steady nature of the global drive [2,3]. As illustrated in Figs. 1(a)–1(d), the violation of Newton's third law is not specific to sedimentation but applies to systems as diverse as colloidal spinners [4–7], driven emulsions [8–10], and swimmer suspensions [11]. Beyond the specifics of fluid mechanics, nonreciprocal couplings rule systems as diverse as self-phoretic colloids [12–14], programmable matter [15,16], dirty plasmas [17], groups of living creatures [18–20], and motile agents [21–23]. Despite a surge of recent efforts, see, e.g., Refs. [16,24–29], the basic principles relating the violation of Newton's third law at the microscopic level to the phase behavior, and mechanics of driven soft matter remains elusive and limited to specific realizations.

In this Letter, we investigate the mechanics of crystals assembled from (self-)driven units defying Newton's third law. We lay out a comprehensive description of their elastic responses, by classifying nonreciprocal microscopic interactions in term of their symmetry under parity transformation. Building on this framework, we then combine theory and simulations to show that driven lattices generically feature a macroscopic response that defies our intuition based on solid mechanics, and host self-propelled dislocations.

Let us consider the overdamped dynamics of a collection of N identical point particles in a homogeneous medium. The particles, located at positions $\mathbf{R}^\nu(t)$, are supposed to interact via pairwise-interaction forces balanced by a local frictional drag $-\zeta\dot{\mathbf{R}}^\nu(t)$. Their equations of motion reduce to the generic form [36]

$$\zeta\dot{\mathbf{R}}^\nu = \sum_{\mu\neq\nu}\mathbf{F}(\mathbf{R}^\mu - \mathbf{R}^\nu), \tag{1}$$

when ignoring the possible nonlinear interplay between local drag and structural deformations [37,38]. In all that follows, we set $\zeta = 1$ without loss of generality. Having ignored the many degrees of freedom of the medium hosting the N particles, we stress that the effective force $\mathbf{F}$ is not constrained to derive from any interaction potential (or free energy). It includes all effective couplings mediated by the soft matrix surrounding the particles. For instance, $\mathbf{F}$ can reflect the hydrodynamic, or phoretic, interactions experienced by particles driven in a viscous fluid [1,11,13], or the elastic forces acting on active inclusions deforming an elastic solid [39–42]. Beyond the specifics of these examples, the N particles can continuously exchange linear and angular momentum with their surrounding environment, thereby alleviating the constraints imposed by Newton's third law. In general, we have (i) $\mathbf{F}(\mathbf{R}^\mu - \mathbf{R}^\nu) \neq -\mathbf{F}(\mathbf{R}^\nu - \mathbf{R}^\mu)$ and (ii) $\mathbf{R}\times\mathbf{F}(\mathbf{R}) \neq \mathbf{0}$. We henceforth refer to forces obeying (i) or (ii) as nonreciprocal forces. To investigate the consequences of force nonreciprocity, we decompose $\mathbf{F}$ on its symmetric and antisymmetric components under parity transformation: $\mathbf{F}(\mathbf{R}) = \mathbf{F}_A(\mathbf{R}) + \mathbf{F}_S(\mathbf{R})$, where the parity-symmetric interactions $[\mathbf{F}_S(-\mathbf{R}) = \mathbf{F}_S(\mathbf{R})]$ contribute to linear momentum exchange with the surrounding medium, while the parity-antisymmetric interactions $[\mathbf{F}_A(-\mathbf{R}) = -\mathbf{F}_A(\mathbf{R})]$ reflect orbital momentum exchange. To gain some intuition, we show two prototypical examples of

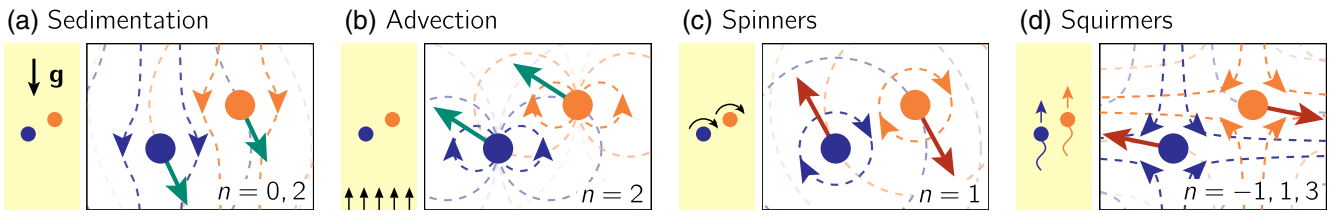

FIG. 1. Hydrodynamic interactions do not obey Newton's third law. We give four examples of nonreciprocal forces between pairs of identical particles driven in a viscous fluid. Parity-symmetric forces (green arrows) correspond to equal drag forces acting on the particles. (a) Two identical particles sedimenting in a viscous fluid. The interaction force field decomposes on the $n = 0, 2$ modes of Eq. (3). (b) Two particles advected in a shallow microfluidic channel interact hydrodynamically via the sole $n = 2$ mode. Parity-antisymmetric forces (red arrows) correspond to opposite drag forces acting on the particles. (c) Two particles spinning in a viscous fluid interact via transverse forces ($n = 1$ mode only). (d) When swimming in the same direction two so-called squirmers interact hydrodynamically via the superposition of forces with $n = -1$, 1, and 3 angular modes [30].

parity-symmetric interactions in Figs. 1(a) and 1(b), and contrast them with two classical examples of antisymmetric hydrodynamic interactions in Figs. 1(c) and 1(d).

We first note that all Bravais lattices correspond to a stationary solution of Eq. (1). Translational invariance indeed implies that nonreciprocal forces result in a homogeneous translation of the lattice at a speed $\mathbf{V}_0 = \sum_{\mu\neq 0} \mathbf{F}_S(\mathbf{R}_0^\mu)$, where $\mathbf{R}_0^\mu$ are the positions in the crystal centered on $\mathbf{R}_0^0 = \mathbf{0}$.

However, nonreciprocal forces typically amplify microscopic fluctuations and destabilize 2D crystalline order. To see this, we address the linear stability of the crystal by considering plane-wave displacements $\mathbf{u}(\mathbf{q}, t)e^{-i\mathbf{q}\cdot\mathbf{R}_0^\nu}$. They satisfy

$$\dot{\mathbf{u}}(\mathbf{q}, t) = (M_A + iM_S) \cdot \mathbf{u}(\mathbf{q}, t) \tag{2}$$

where the real matrices M_A and M_S, respectively, depend on $\nabla\mathbf{F}_A$ and $\nabla\mathbf{F}_S$. As thoroughly discussed in Supplemental Material (SM) [30], we first note that the two eigenvalues of iM_S cannot be both real and negative: phonons cannot be overdamped. Parity-symmetric forces can, however, power the free propagation of sound waves as experimentally observed in driven microfluidic crystals interacting via the symmetric forces sketched in Fig. 1(b), see [8–10]. The case of parity-antisymmetric forces is more subtle. However, in a host of experimentally relevant situations, these forces are divergenceless, such as hydrodynamic interactions induced by potential flows, phoretic interactions [12,14], and transverse frictional forces [7,28,43]. The condition $\boldsymbol{\nabla} \cdot \mathbf{F}_A = 0$ implies $\mathrm{tr}(M_A) = 0$. The eigenvalues of M_A are then either opposite and real or pure imaginary numbers. Therefore, F_A either destabilizes 2D crystals or powers the propagation of free phonons, in agreement with the phenomenology reported in colloidal spinner crystals [7,28,43]. In sum, regardless of their microscopic origin, nonreciprocal forces are typically unable to self-organize identical units into a stable crystal state.

To understand how nonreciprocal forces modify the mechanics of elastic crystals, it is useful to classify the interactions with respect to their angular symmetries. In all that follows we consider a generic class of forces which we decompose in a multipolar expansion as

$$\mathbf{F}(\mathbf{R} = re^{i\theta}) = \sum_n f_n(r)e^{i(n\theta-\alpha_n)}, \tag{3}$$

where we use the complex-number representation for the 2D vectors. Forces are parity-symmetric when n is even, and antisymmetric when n is odd. Given this simple decomposition Newton's third law would reduce the sum in Eq. (3) to its sole $n = 1$ mode, and imply $\alpha_1 = 0$. At lowest orders, nonreciprocal interactions correspond to forces with $n = 1$, $\alpha_1 = \pi/2$, and $n = 2$. They are realized by two paradigmatic examples of driven soft matter. The parity-odd case $n = 1$, $\alpha_1 = \pi/2$, corresponds to the forces experienced by collections of active or driven spinners interacting either by near-, or far-field hydrodynamic interactions in a viscous fluid, see Fig. 1(c) and, e.g., Refs. [4–6,44–46]. Similarly, the parity-even case $n = 2$ corresponds to the standard dipolar flows ruling the interactions between foams, emulsions, or colloids uniformly driven in shallow channels, see Fig. 1(b) and, e.g., Refs. [8,47–49].

We focus here on perfect hexagonal lattices, and compute the stresses σ and body forces $\mathcal{F}$ resulting from linear deformations. In line with our intuition based on equilibrium solids, we show below that parity-odd interactions convert deformations into stresses. However, parity-even forces do not cancel one another. As a result, deformations generically produce net forces.

Without loss of generality we define the real space displacement field $\mathbf{u}(\mathbf{r})$, and decompose the deformations tensor $D_{ij} = \partial u_i/\partial x_j$, on the basis defined by the pure dilation (τ_{ij}^δ), rotation (τ_{ij}^ω), and two orthogonal shear modes ($\tau_{ij}^{s_1}$ and $\tau_{ij}^{s_2}$): $D_{ij} = D_\delta\tau_{ij}^\delta + D_\omega\tau_{ij}^\omega + D_{s_1}\tau_{ij}^{s_1} + D_{s_2}\tau_{ij}^{s_2}$ [see Fig. 2(b)].

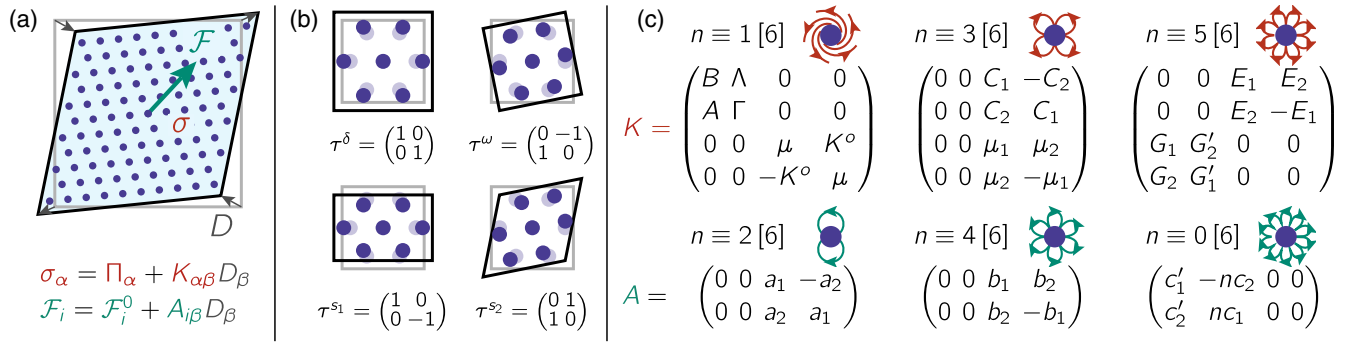

FIG. 2. Mechanics of elastic lattices challenged by nonreciprocal interactions. (a) When a hexagonal lattice undergoes a deformation, parity-antisymmetric forces induce a stress σ (red) that can be computed using the Irving-Kirkwood formula [Eq. (5)]. The macroscopic response to a deformation D reads $\sigma_\alpha = \Pi_\alpha + K_{\alpha\beta} D_\beta$ where α, β denote the elementary stress and deformation modes defined in (b) and Π is a so-called prestress supported by the crystal even in absence of any deformations. In the case of parity-symmetric interactions, a deformation D induces a net force $\mathcal{F}$ defined as the net force experienced by any test particle (green arrow). $\mathcal{F}$ and D are related by the linear yet noninvertible relation $\mathcal{F}_i = \mathcal{F}_i^0 + A_{i\beta} D_\beta$ where $i = x, y$. The six possible structures for the matrices K and A are given in (c). (b) Elementary modes of 2D deformations (and stresses). τ^δ corresponds to a dilation (isotropic pressure), τ^ω to a rotation (torque), while τ^{s_1} and τ^{s_2} are the two pure-shear deformations (shear stresses). (c) On a hexagonal lattice, parity-antisymmetric interactions define three classes of stress-strain relations. These constitutive relations are determined by the angular symmetry of the interactions ($n \equiv 1, 3, 5[6]$ where "[6]" stands for "modulo 6"), see Eq. (3). The prestresses Π are given: $\Pi = (P_\delta, T_\omega, 0, 0)$ when $n \equiv 1[6]$, $\Pi = 0$ when $n \equiv 3[6]$, and $\Pi = (0, 0, S_1, S_2)$ when $n \equiv 5[6]$. Parity-symmetric interactions define three classes of force-strain relations determined by the angular symmetry of the interactions ($n \equiv 2, 4, 0[6]$). The three possible constitutive relations correspond to the three possible structures of the matrix A. A net force $\mathcal{F}_i^0$ can exist even in the absence of deformation under the action of nonreciprocal interactions when $n \equiv 0[6]$, it is given by $\mathcal{F}_i^0 = (c_1, c_2) \neq 0$. The analytic expression of all material parameters are expressed in terms of the microscopic interactions both for parity-antisymmetric and symmetric forces in the SM [30].

Parity even interactions.—To illustrate the counterintuitive mechanics induced by parity even forces, we first focus on the minimal example of interactions having a dipolar symmetry [$n = 2$, see Fig. 1(b)]. Computing the force $\mathcal{F}$ acting on a test particle in a deformed hexagonal lattice, we find that the force components ($\mathcal{F}_i$) depend linearly on deformation (D_{ij}):

$$\mathcal{F} = K_2 \begin{pmatrix} \cos\alpha_2 & \sin\alpha_2 \\ -\sin\alpha_2 & \cos\alpha_2 \end{pmatrix} \begin{pmatrix} D_{s_1} \\ D_{s_2} \end{pmatrix}, \tag{4}$$

where $K_2 = \sum_{\mu \neq 0} [f_2(R_0^\mu) + R_0^\mu f_2'(R_0^\mu)/2]$. The consequences of Eq. (4) are clear. Having in mind a colloidal crystal driven in a 2D fluid, say in the x direction (leading to $\alpha_2 = 0$), longitudinal shear deformations (D_{s_1}) accelerate or slow down translational motion whereas shearing the lattice at a 45° angle (D_{s_2}) results in a net drift in the direction transverse to the applied drive. Rotation and dilation do not yield any net force. We emphasize that this atypical response relating strain to body forces is linear but not invertible. It therefore violates any form of macroscopic reciprocity [16,24]. Uniform deformations cause net uniform forces, but applying a homogeneous force merely translates the crystal leaving its inner structure unaltered. The emergence of net body forces from crystal deformations is not specific to dipolar interactions, but generically emerges from nonreciprocal forces even under parity transformations. In Fig. 2(c), we show the only three possible constitutive relations in crystals enjoying a sixfold symmetry defined by the response matrix A: $\mathcal{F}_i = \mathcal{F}_i^0 + A_{i\beta} D_\beta$ where the implicit summation (β index) is done over the four deformation modes.

Parity-odd forces.—The case of parity-odd forces is more familiar. Let us start again with a simple example, when the microscopic forces are isotropic [$n = 1$, $\alpha_1 \neq 0$, see Fig. 1(c)], our hexagonal lattice realizes a typical example of an odd-elastic solid introduced in Ref. [28] and exemplified in Ref. [7]. Deformations do not yield body force but build up a net stress which we can readily compute using the Irving-Kirkwood formula [50–52],

$$\sigma_{ij} = \frac{1}{V} \sum_{\mu \neq 0} R_i^\nu F_j(\mathbf{R}^\mu), \tag{5}$$

where the summation excludes the particle at the origin and V is the volume of the unit cell. Decomposing the stress on the dilation, rotation, and two shear modes $(\sigma_\delta, \sigma_\omega, \sigma_{s_1}, \sigma_{s_2})$ we then find the constitutive relation

$$\begin{pmatrix} \sigma_\delta \\ \sigma_\omega \\ \sigma_{s_1} \\ \sigma_{s_2} \end{pmatrix} = \begin{pmatrix} P_\delta \\ T_\omega \\ 0 \\ 0 \end{pmatrix} + \begin{pmatrix} B & 0 & 0 & 0 \\ A & 0 & 0 & 0 \\ 0 & 0 & \mu & K^o \\ 0 & 0 & -K^o & \mu \end{pmatrix} \begin{pmatrix} D_\delta \\ D_\omega \\ D_{s_1} \\ D_{s_2} \end{pmatrix}, \tag{6}$$

where the analytic expressions of all material parameters are presented in SM [30] together with an alternative geometrical derivation of σ. Two comments are in order. First, the undeformed crystal can support both a nonzero pressure P_δ and a nonzero odd stress T_ω, viz., a net torque density resulting from the angular momentum exchange with the surrounding medium. This result confirms early phenomenological theories, simulations, and recent experiments conducted on colloidal and granular spinners [6,53–55]. Second, we find that the bulk and shear moduli (B and μ) both vanish for purely transverse forces ($\alpha_1 = \pi/2$), whereas odd elasticity (coefficients A and K^o) emerges when $\alpha_1 \neq 0$. Remarkably, in hexagonal lattices all microscopic interactions satisfying $n \equiv 1 \pmod 6$ yield the same macroscopic elastic response, which expands the existence of odd elastic solids beyond the specifics of purely transverse forces. More generally, we summarize our results obtained for all odd n in Fig. 2(c), and show the only three possible affine constitutive relations of nonreciprocal hexagonal crystals. When $|n| \geq 3$ elasticity is not isotropic anymore, even in hexagonal lattices. We also note that when $n \equiv 5 \pmod 6$ undeformed lattices support a net shear stress $(\sigma_{s_1}, \sigma_{s_2}) = (S_1, S_2)$ mirroring the odd stress of chiral crystals [6,54,55].

Our continuum mechanics picture provides an effective platform to go beyond linear deformations, and address the impact of dislocations on the crystal structure and dynamics. To gain some insight, we first solve Eq. (1) numerically using periodic boundary conditions, for a hexagonal lattice deformed by two maximally separated dislocations of opposite Burgers vector (periodic boundary conditions require a zero net topological charge). The numerical methods are detailed in SM [30]. We investigate separately the impact of each angular mode. Remarkably, Supplemental Material, Video 1 [30] reveals that the competition between nonreciprocal forces and elasticity turns dislocations into self-propelled singularities. Figure 3(b) illustrates the gliding motion of dislocations powered by dipolar ($n = 2$) interactions.

To explain this spontaneous motion in the direction of the Burgers vector $\mathbf{b}$, we consider an isolated dislocation at the origin of an isotropic elastic solid [$B \neq 0$ and $\mu \neq 0$ in Eq. (6)]. In the case of parity-odd forces, the induced internal extra stress Π, see Fig. 2, results in a net Peach-Koehler force $F_i^{\mathrm{PK}} = \epsilon_{ij}\Pi_{kj}b_k$, computed in SM [30]. When $\mathbf{b} = b\mathbf{e}_1$, the glide component of the force takes a compact form when $n \equiv 1, 5 \pmod 6$:

$$F^{\mathrm{PK}}_{\mathrm{glide}}(n=1) = -T_\omega b, \qquad F^{\mathrm{PK}}_{\mathrm{glide}}(n=5) = S_2 b. \quad (7)$$

The case $n = 3$ deserves a separate study [30], which accounts for the local rotation of the crystal orientation.

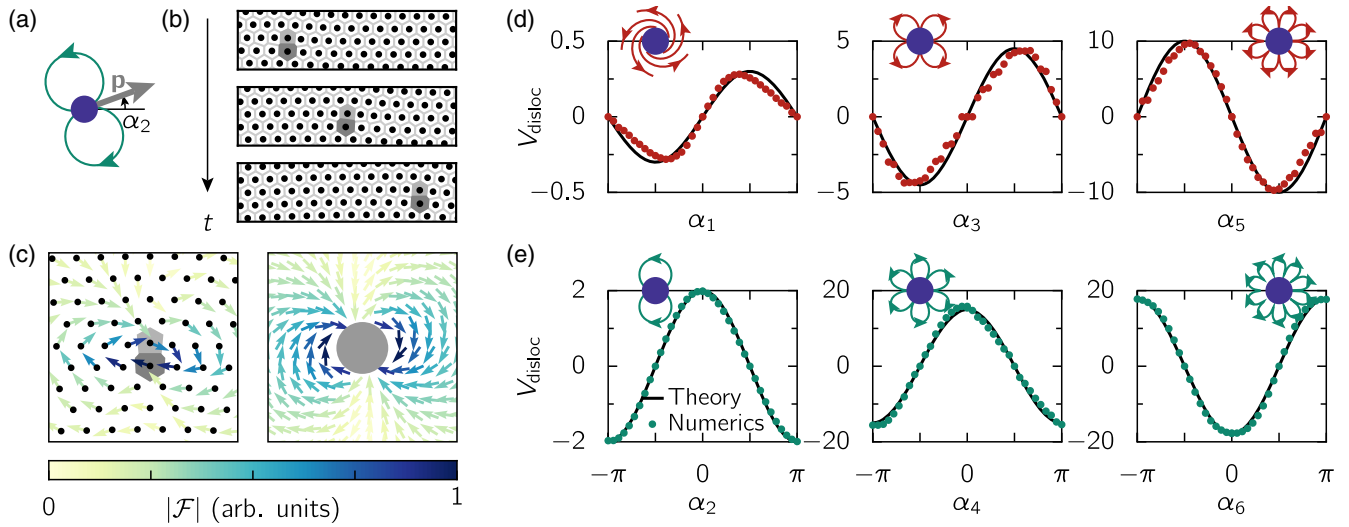

FIG. 3. Nonreciprocal interactions power dislocation glide. In our numerical simulations [30], we choose the nonreciprocal interactions to correspond to pure multipoles. When $n \geq 2$, $f_n(r) = 1/r^n$ [see Eq. (3)]. The case $n = 2$ then corresponds to hydrodynamic interactions in shallow channels. For $n = 1$, we arbitrarily choose $f_1(r) = e^{-r^2/2}$ to reflect the short range coupling between colloidal spinners. Furthermore, the crystal is stabilized by reciprocal interactions $\mathbf{F}(\mathbf{r}) = -A_{\mathrm{rep}}\mathbf{r}/\|\mathbf{r}\|^5$ (dipole-dipole repulsion). (a) Sketch of dipolar field ($n = 2$) induced by a given particle. α_2 is the phase of mode $n = 2$ and $\mathbf{p} = (\cos\alpha_2, \sin\alpha_2)$. (b) Glide of a dislocation in a crystal. The nonreciprocal interactions correspond to $n = 2$, $\alpha_2 = 20°$ ($A_{\mathrm{rep}} = 10$). The three snapshots correspond to $t = 0$, 0.25, and 0.5. (c) Left: numerical computation of the forces on the particles induced by dipolar pairwise interactions ($\alpha_2 = 20°$). Right: theoretical prediction for the force field according to Eq (8), for the same microscopic parameters. (d) The variations of the gliding speed of a dislocation with the phase α_n measured from our numerical simulations (red dots) are in excellent agreement with our theoretical predictions (black solid line). From left to right $n = 1$, 3, and 5 ($A_{\mathrm{rep}} = 1$, 10, 50). (e) Same plots as in (d) in the case of parity-even forces. From left to right $n = 2$, 4, and 6 ($A_{\mathrm{rep}} = 10$, 20, 50).

Beyond the existence of a nonvanishing Peach-Koehler force, our theoretical predictions quantitatively account for the variations of the dislocation speed as a function of the microscopic force's phase α_n shown in Fig. 3(d). Our finding confirms and generalizes the experimental and numerical results reported in odd colloidal crystals ($n = 1$) [7].

The influence of parity-even forces, is yet again more subtle as they do not translate in macroscopic stresses but net forces. This essential difference requires expanding the conventional Peach-Koehler picture. We can gain some intuition by looking at the symmetry of the microscopic-force distribution around an isolated dislocation when perturbed by dipolar forces ($n = 2$), see Fig. 3(c). It clearly reveals a simple shear component, which is correctly captured by our continuum theory [Eq. (4)] [30]. Using the strain field around an isolated dislocation [56,57], the force field takes the form

$$\mathcal{F}(r,\theta) = \mathcal{F}_0 \frac{\mathbf{b}\cdot\mathbf{r}}{r^2}\begin{pmatrix} \sin(2\theta-\alpha_2) \\ -\cos(2\theta-\alpha_2) \end{pmatrix}, \tag{8}$$

where $\mathcal{F}_0 = -[K_2(1+\nu)]/4\pi$, and $\nu = (B-\mu)/(B+\mu)$. We can then define an effective Peach-Koehler force acting on the dislocation core as $F_i^{\mathrm{PK}} = \epsilon_{ij}\partial_k \mathcal{F}_j b_k$. To evaluate it, we need to regularize the force gradient at $r = 0$. As detailed in SM [30], we evaluate $\mathbf{F}^{\mathrm{PK}}$ as a weighted integral over a circle of radius b around the dislocation core. We finally find

$$\mathbf{F}^{\mathrm{PK}} = \frac{1}{4}\mathcal{F}_0 \mathbf{p}, \tag{9}$$

where $\mathbf{p} = (\cos\alpha_2, \sin\alpha_2)$ is the vector defining the dipole orientation [Fig. 3(a)]. This expression indicates that nonreciprocal dipolar forces can sustain the gliding motion of dislocations having a Burgers vector making a finite angle with $\mathbf{p}$. To further confirm this prediction, we use our numerical simulations and plot the glide velocity as a function of the angle α_2. Figure 3(e) shows a remarkable agreement with our effective elastic theory predicting a speed proportional to $\cos\alpha_2$. As a last result, we stress that beyond the specifics of dipolar forces, the emergent Peach-Koehler forces evaluated at the continuum level correctly account for the variations of the dislocation speed measured in our numerical simulations whatever the angular symmetry of the nonreciprocal forces [Fig. 3(e)].

We have elucidated the relations between the microscopic symmetries of nonequilibrium interactions and the macroscopic response of driven lattices. From a practical perspective, the systematic classification summarized in Fig. 2 suggests effective strategies to design active metamaterials having mechanical properties out of reach of equilibrium systems. From a fundamental perspective, our findings immediately raise three basic questions: how does dislocation motility redefine the plastic flows, fracture, and melting of driven and active crystals?

We thank E. Billilign, Y. Ganan, W. T. M Irvine, M. Le Blay, and V. Vitelli for invaluable discussions and suggestions. This work was partly supported by IDEX LYON grant ToRe and ANR grant WTF.

*alexis.poncet@ens-lyon.fr
†denis.bartolo@ens-lyon.fr

[1] J. Happel and H. Brenner, *Low Reynolds Number Hydrodynamics: With Special Applications to Particulate Media* (Springer, Dordrecht, 1983), Vol. 1, ISBN 978-90-247-2877-0.
[2] E. Guazzelli and J. Hinch, Annu. Rev. Fluid Mech. **43**, 97 (2011).
[3] S. Ramaswamy, Adv. Phys. **50**, 297 (2001).
[4] J. Yan, S. C. Bae, and S. Granick, Soft Matter **11**, 147 (2015).
[5] A. P. Petroff, X.-L. Wu, and A. Libchaber, Phys. Rev. Lett. **114**, 158102 (2015).
[6] V. Soni, E. S. Bililign, S. Magkiriadou, S. Sacanna, D. Bartolo, M. J. Shelley, and W. T. Irvine, Nat. Phys. **15**, 1188 (2019).
[7] E. S. Bililign, F. B. Usabiaga, Y. A. Ganan, A. Poncet, V. Soni, S. Magkiriadou, M. J. Shelley, D. Bartolo, and W. T. M. Irvine, Nat. Phys. (2021), 10.1038/s41567-021-01429-3.
[8] T. Beatus, T. Tlusty, and R. Bar-Ziv, Nat. Phys. **2**, 743 (2006).
[9] T. Beatus, R. Bar-Ziv, and T. Tlusty, Phys. Rev. Lett. **99**, 124502 (2007).
[10] N. Desreumaux, N. Florent, E. Lauga, and D. Bartolo, Eur. Phys. J. E **35**, 68 (2012).
[11] E. Lauga, *The Fluid Dynamics of Cell Motility* (Cambridge University Press, Cambridge, England, 2020), Vol. 62.
[12] R. Soto and R. Golestanian, Phys. Rev. Lett. **112**, 068301 (2014).
[13] S. Saha, R. Golestanian, and S. Ramaswamy, Phys. Rev. E **89**, 062316 (2014).
[14] J. Agudo-Canalejo and R. Golestanian, Phys. Rev. Lett. **123**, 018101 (2019).
[15] F. A. Lavergne, H. Wendehenne, T. Bäuerle, and C. Bechinger, Science **364**, 70 (2019).
[16] M. Fruchart, R. Hanai, P. B. Littlewood, and V. Vitelli, Nature (London) **592**, 363 (2021).
[17] A. V. Ivlev, J. Bartnick, M. Heinen, C.-R. Du, V. Nosenko, and H. Löwen, Phys. Rev. X **5**, 011035 (2015).
[18] A. Cavagna and I. Giardina, Annu. Rev. Condens. Matter Phys. **5**, 183 (2014).
[19] M. Moussaïd, D. Helbing, and G. Theraulaz, Proc. Natl. Acad. Sci. U.S.A. **108**, 6884 (2011).
[20] A. Filella, F. Nadal, C. Sire, E. Kanso, and C. Eloy, Phys. Rev. Lett. **120**, 198101 (2018).
[21] T. Vicsek, A. Czirók, E. Ben-Jacob, I. Cohen, and O. Shochet, Phys. Rev. Lett. **75**, 1226 (1995).
[22] Q.-s. Chen, A. Patelli, H. Chaté, Y.-q. Ma, and X.-q. Shi, Phys. Rev. E **96**, 020601(R) (2017).

[23] L. P. Dadhichi, J. Kethapelli, R. Chajwa, S. Ramaswamy, and A. Maitra, Phys. Rev. E **101**, 052601 (2020).
[24] C. Coulais, D. Sounas, and A. Alù, Nature (London) **542**, 461 (2017).
[25] M. Brandenbourger, X. Locsin, E. Lerner, and C. Coulais, Nat. Commun. **10**, 4608 (2019).
[26] L. Barberis and F. Peruani, J. Chem. Phys. **150**, 144905 (2019).
[27] S. Saha, J. Agudo-Canalejo, and R. Golestanian, Phys. Rev. X **10**, 041009 (2020).
[28] C. Scheibner, A. Souslov, D. Banerjee, P. Surowka, W. T. Irvine, and V. Vitelli, Nat. Phys. **16**, 475 (2020).
[29] S. A. Loos and S. H. Klapp, New J. Phys. **22**, 123051 (2020).
[30] See Supplemental Material http://link.aps.org/supplemental/10.1103/PhysRevLett.128.048002 for detailed computations and numerical methods, which includes Refs. [31–35].
[31] J. M. Crowley, Phys. Fluids **19**, 1296 (1976).
[32] M. Doi and S. F. Edwards, *The Theory of Polymer Dynamics* (Oxford University Press, New York, 1988), Vol. 73.
[33] P. Oswald, *Rheophysics* (Cambridge University Press, Cambridge, England, 2009).
[34] W. T. M. Irvine, A. D. Hollingsworth, D. G. Grier, and P. M. Chaikin, Proc. Natl. Acad. Sci. U.S.A. **110**, 15544 (2013).
[35] D. Frenkel and B. Smit, *Understanding Molecular Simulation: From Algorithms to Applications* (Elsevier, New York, 2001), Vol. 1.
[36] The dynamics also reduces to Eq. (1) when a constant driving force $\mathbf{F}_0$ acts on all particles (by setting $\mathbf{R} \to \mathbf{R} - \mathbf{F}_0 t$).
[37] R. Lahiri and S. Ramaswamy, Phys. Rev. Lett. **79**, 1150 (1997).
[38] R. Chajwa, N. Menon, S. Ramaswamy, and R. Govindarajan, Phys. Rev. X **10**, 041016 (2020).
[39] S. Ramaswamy, J. Toner, and J. Prost, Phys. Rev. Lett. **84**, 3494 (2000).
[40] N. Kumar, H. Soni, S. Ramaswamy, and A. Sood, Nat. Commun. **5**, 4688 (2014).
[41] S. Ramananarivo, E. Ducrot, and J. Palacci, Nat. Commun. **10**, 3380 (2019).
[42] R. K. Gupta, R. Kant, H. Soni, A. K. Sood, and S. Ramaswamy, arXiv:2007.04860.
[43] T. H. Tan, A. Mietke, H. Higinbotham, J. Li, Y. Chen, P. J. Foster, S. Gokhale, J. Dunkel, and N. Fakhri, arXiv:2105.07507.
[44] K. Yeo, E. Lushi, and P. M. Vlahovska, Phys. Rev. Lett. **114**, 188301 (2015).
[45] N. Oppenheimer, D. B. Stein, and M. J. Shelley, Phys. Rev. Lett. **123**, 148101 (2019).
[46] Z. Shen and J. S. Lintuvuori, Phys. Rev. Lett. **125**, 228002 (2020).
[47] N. Desreumaux, J.-B. Caussin, R. Jeanneret, E. Lauga, and D. Bartolo, Phys. Rev. Lett. **111**, 118301 (2013).
[48] I. Shani, T. Beatus, R. H. Bar-Ziv, and T. Tlusty, Nat. Phys. **10**, 140 (2014).
[49] D. Mondal, A. G. Prabhune, S. Ramaswamy, and P. Sharma, eLife **10**, e67663 (2021).
[50] J. H. Irving and J. G. Kirkwood, J. Chem. Phys. **18**, 817 (1950).
[51] J. Z. Yang, X. Wu, and X. Li, J. Chem. Phys. **137**, 134104 (2012).
[52] K. Klymko, D. Mandal, and K. K. Mandadapu, J. Chem. Phys. **147**, 194109 (2017).
[53] J. Dahler and L. Scriven, Nature (London) **192**, 36 (1961).
[54] J.-C. Tsai, F. Ye, J. Rodriguez, J. P. Gollub, and T. C. Lubensky, Phys. Rev. Lett. **94**, 214301 (2005).
[55] B. C. van Zuiden, J. Paulose, W. T. Irvine, D. Bartolo, and V. Vitelli, Proc. Natl. Acad. Sci. U.S.A. **113**, 12919 (2016).
[56] L. D. Landau and E. M. Lifshitz, *Theory of Elasticity* (Pergamon Press, Oxford New York, 1986).
[57] L. Braverman, C. Scheibner, B. VanSaders, and V. Vitelli, Phys. Rev. Lett. **127**, 268001 (2021).